

Mid-Rapidity Identified Hadron A_{LL} in
Polarized Proton-Proton Collisions at 200
GeV at STAR

William Leight

Massachusetts Institute of Technology

For the  Collaboration

Measurement of neutral pion double-helicity asymmetry in data from 200 gev polarized proton-proton collisions taken by the star experiment

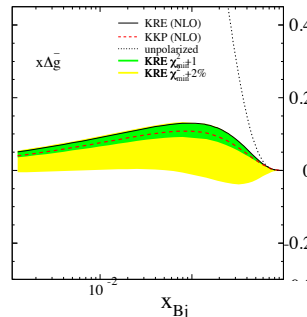
The Proton Spin and ΔG

The proton spin can be written as $\frac{1}{2} = \frac{1}{2}\Delta\Sigma + L_q + \Delta G + L_g$.

Polarized DIS measurements indicate that $\Delta\Sigma$ accounts for only ~30% of the proton spin.

$$\Delta G(Q^2) = \int_0^1 dx (g^+(x, Q^2) - g^-(x, Q^2))$$

$\Delta g(x)$ can be measured in polarized DIS but with large uncertainties.



D. de Florian, G.A. Navarro, and R. Sassot, *AIP Conf. Proc.*, 792:921-924, 2005

2

We know that the proton spin is $\frac{1}{2}$, and we know that the proton is made up of quarks and gluons, so the proton spin must arise from the spins and orbital angular momenta of the quarks and gluons. We can measure the quark spin contribution to the proton spin in polarized deep inelastic scattering experiments, which indicate that the quark polarization delta sigma accounts for about 30% of the proton spin, but what about the gluon spin contribution delta g, the integral over bjorken x of the polarized gluon pdf? Delta g can also be measured in polarized dis, but only indirectly through scaling violations, resulting in large uncertainties, as can be seen in this plot showing a global fit of delta g from polarized dis results.

ΔG in Polarized p-p Collisions

ΔG can be accessed in longitudinally polarized proton-proton collisions through the observable A_{LL} , defined in the general case as

$$A_{LL} = \frac{\sigma_{++} - \sigma_{+-}}{\sigma_{++} + \sigma_{+-}}$$

For the specific case of π^0 production, A_{LL} can be factorized into parton distribution functions, cross-sections, and fragmentation functions as follows:

$$A_{LL} = \frac{\sum_{f=q,\bar{q},g} \Delta f_a \times \Delta f_b \times d\Delta\hat{\sigma}^{f_a f_b \rightarrow f X} \times D_f^{\pi^0}}{\sum_{f=q,\bar{q},g} f_a \times f_b \times d\hat{\sigma}^{f_a f_b \rightarrow f X} \times D_f^{\pi^0}}$$

If one (or both) of the partons f_a and f_b is a gluon, A_{LL} directly accesses $\Delta g(x, Q^2)$.

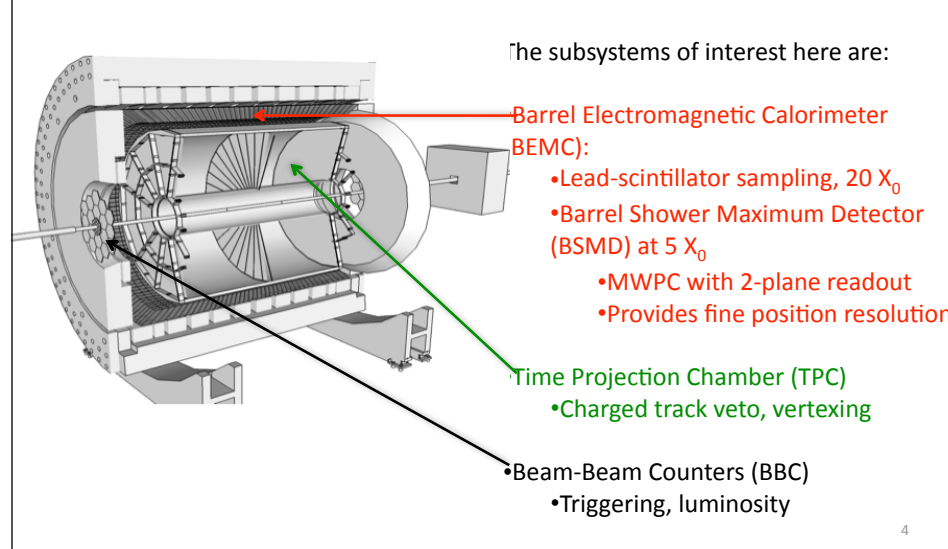
Experimentally, A_{LL} is calculated as $A_{LL} = \frac{1}{P_1 P_2} \frac{N^{++} - RN^{+-}}{N^{++} + RN^{+-}}$

where the P 's are the beam polarizations and R is the ratio of the luminosities in the two helicity configurations.

3

We'd like to be able to access delta g directly, through longitudinally polarized pp collisions, for which we use the observable a_{LL} , defined as the difference between the cross-section for some process with the proton spins aligned and with the spins anti-aligned divided by the total cross-section. Theoretically, we can factor a_{LL} into a product of parton distribution functions (polarized and unpolarized), hard scattering cross-sections, and fragmentation functions for our process (in this case, neutral pion production): if one or both of the partons f_a and f_b in the hard scattering is a gluon, a_{LL} directly access delta-g. Experimentally, because the factors that we use to transform a yield into a cross-section cancel out in the ratio, we calculating a_{LL} directly from the neutral pion spin-aligned and anti-aligned yields, n^{++} and n^{+-} , with the latter normalized by the relative luminosity factor and the whole divided by the product of the beam polarizations.

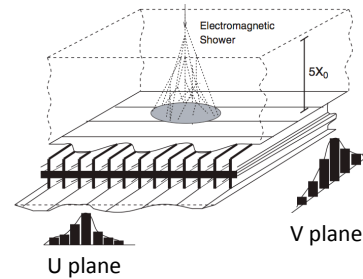
The STAR Detector



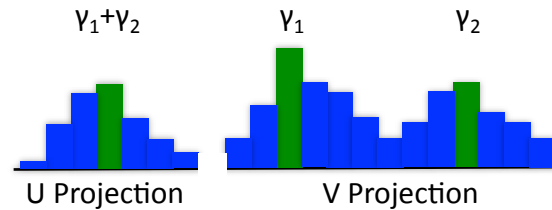
Here's a picture of the star detector: the main subsystem of interest for this analysis is the barrel electromagnetic calorimeter, a lead-scintillator sampling calorimeter that has full phi coverage and eta coverage from -1 to 1. the benc is 20 radiation lengths deep: at a depth of about 5 radiation lengths is a shower maximum detector, a multi-wire proportional chamber with 2-plane readout that provides fine position resolution. Also used are the time projection chamber, which provides charged particle tracking and so is used for a charged track veto and for vertexing, and the beam-beam counters, which provide some triggering and luminosity measurements.

BSMD Clustering

Pions are reconstructed from the $\pi^0 \rightarrow \gamma\gamma$ decay channel. Photons leave energy deposits in the two planes of the BSMD (see cartoon at right): an algorithm takes BSMD energy deposits and constructs clusters from the strips separately in each plane (see cartoon below). Clusters are based on seed strips, which are above an ADC threshold and have more energy than the strips on either side.



Example: $\pi^0 \rightarrow \gamma_1 \gamma_2$



Once clusters are found and the charged track veto is applied, photon candidates are constructed by combining clusters in one plane with all sufficiently close clusters in the other plane.

Neutral pions are reconstructed from the $\pi^0 \rightarrow \gamma\gamma$ decay channel: because of the large size of the calorimeter towers, $.05 \times .05$ in η - ϕ , they can separate decay photons only at low energies, so pion reconstruction starts in the shower-max detector. In the upper right is a cartoon of an electromagnetic shower in the bsmd, leaving, in the ideal gauss, roughly gaussian energy deposits in the strips of each plane. The pion-finding algorithm assigns strips to clusters in each plane separately: an example is shown in the lower left, where in the u plane the two photons overlap too much to be distinguished, but in the v plane are easily separable, allowing the pion to be reconstructed. Once the clusters have been found, the charged track veto is applied, and then photon candidates are constructed by combining clusters in the u plane with all the clusters in the v plane that are close enough that it's plausible that they arose from the same photon.

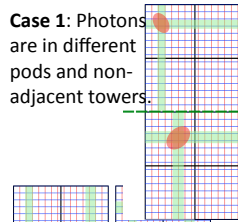
Detector Fake Pions

Pion candidates are formed by taking all possible combinations of photon candidates. They are then sorted by their decay topology in the BEMC; different decay topologies have different methods of calculating energy and so invariant mass.

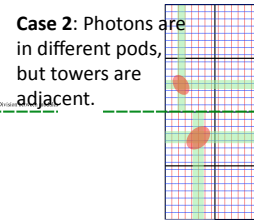
Decay Photon

BSMD Cluster

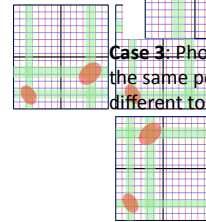
Case 1: Photons are in different pods and non-adjacent towers.



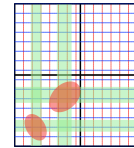
Case 2: Photons are in different pods, but towers are adjacent.



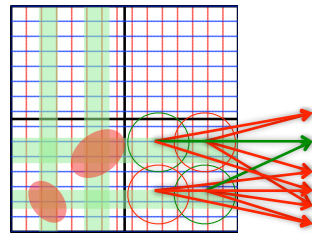
Case 3: Photons in the same pod but different towers.



Case 4: Photons are in the same tower.



Pion Decay Example



In cases 3 and 4, overlapping BSMD clusters create detector fake pions. At left, one genuine pion gives rise to five fake pion candidates that must be removed.

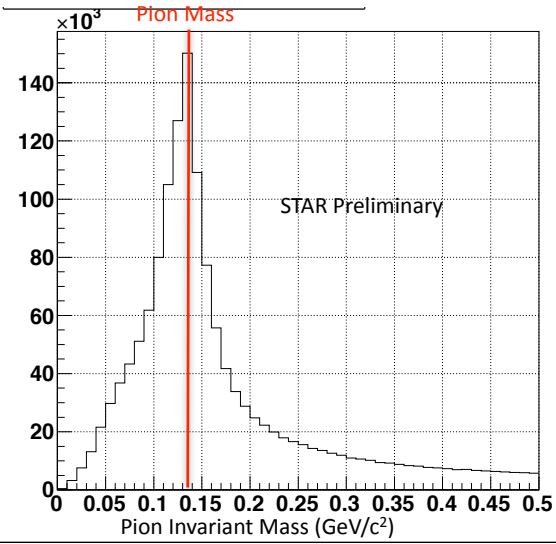
In addition to removing fakes, other cuts are applied, including pion $p_T > 4$.

6

Then pion candidates are formed by taking all possible combinations of photon candidates. It's useful to sort the pion candidates by the way they decay in the calorimeter towers: this is helpful in calculating the candidate energy, since the towers provide the energy measurement, and also in identifying if we need to look for detector fake pions. Here are shown cartoons of each of the four decay types (the orange blobs are the decay photons, the green bands the bsmd clusters): the main distinction, though, is between the first two cases, in which the bsmd clusters of different photons don't overlap, and the second two cases, in which they do. An example of what happens when clusters from different photons overlap is shown in the lower left: in addition to reconstructing the true photons, we also reconstruct two fake photons which are composed of one cluster from one photon and the cluster in the opposite plane from the other photon. These four photons then become six pions, thanks to combinatorics, of which only one, indicated by green arrows, is the true pion, and the other five (red arrows) are fakes. Luckily, we can use the same geometry that creates these fake pions to get rid of them. Once the fakes are removed, some additional cuts are applied, of which the main one is the requirement that the pion candidate have $p_T > 4$.

Invariant Mass Distribution

High-tower and jet-patch (1.0×1.0 in η - ϕ) triggers are used
Run 9 pp200: $\sim 14 \text{ pb}^{-1}$ at an average longitudinal polarization of $\sim 59\%$



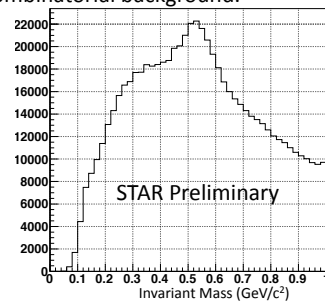
This results in this invariant mass distribution: the neutral pion invariant mass of .135 Gev is indicated by the red line.

Backgrounds

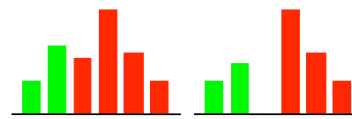
Combinatorial Background

Some pion candidates will be formed from uncorrelated photons. This background is modeled by mixing data events, rotated so that their jet axes align.

Most combinatorial background candidates have photons in non-adjacent towers: above the p_T cut of 4 GeV such candidates are rarely signal, enabling us to remove most combinatorial background.

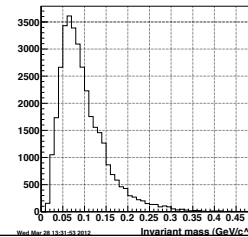


Split-Photon Background



The other main source of background arises from photons which are artificially split in half by bad BSMC strips (cartoon on right, where the missing strip is bad) or random fluctuations (cartoon on left).

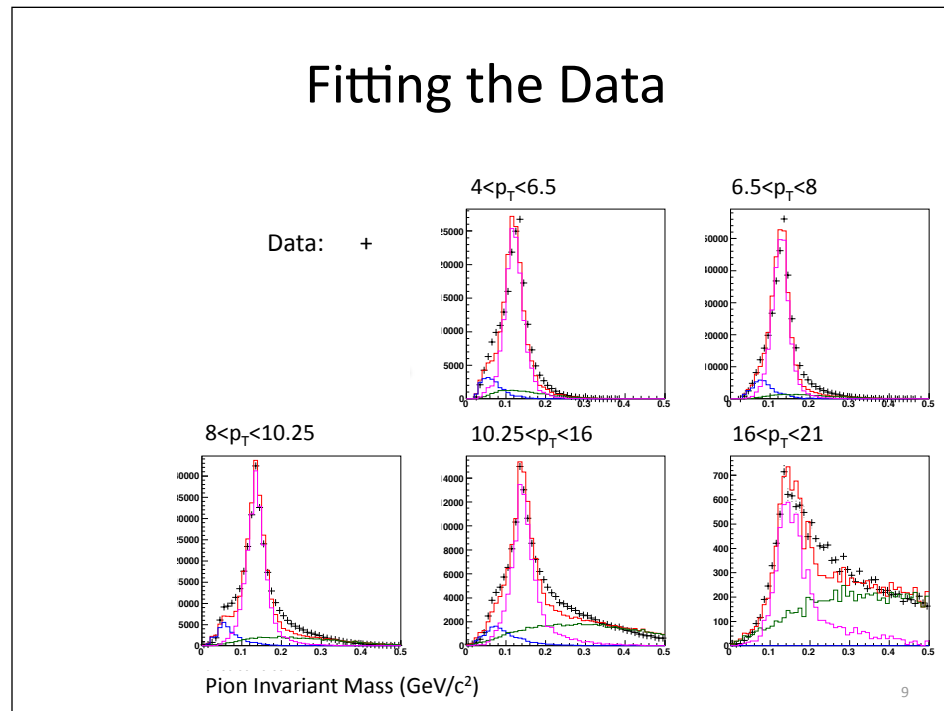
The split-photon background is modeled by simulating single photons in the detector.



8

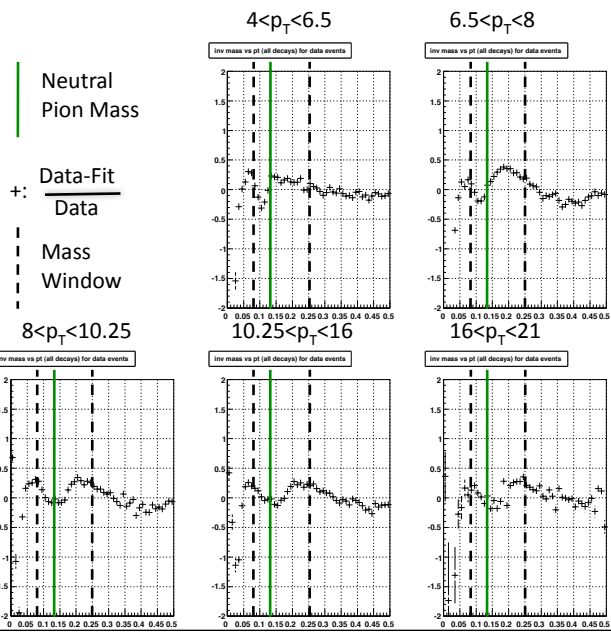
However, there two backgrounds that we still have to deal with. The first is the combinatorial background, which comes from combining uncorrelated photons: we model it by creating pion candidates from photons which we know are uncorrelated because they come from different events. Additionally, we can eliminate a big chunk of this background: most of it consists of pion candidates whose decay photons do not fall into adjacent towers, and above our p_T cutoff of 4 GeV such candidates are essentially never signal, as you can see in this plot where a pion peak is not visible but an eta peak is. The other background is a detector background, arising from clusters in the bsmc being reconstructed as two, either because a bsmc strip had problems (on right) or the energy deposited in a bsmc strip fluctuated high (on left). This background is modeled by propagating photons through the detector and calculating the invariant mass of the “pions” that are reconstructed.

Fitting the Data



Once we have the backgrounds modeled, we can try to see how well we can describe the data in terms of them and the simulated pion peak (obtained from full pp collision simulations). We split the data into five p_T bins, then allow the normalizations of the combinatorial background, split-photon background, and simulated signal peak to vary independently: their sum is the fit to the data, with reasonably good results, though there is some disagreement at the shoulders of the peak.

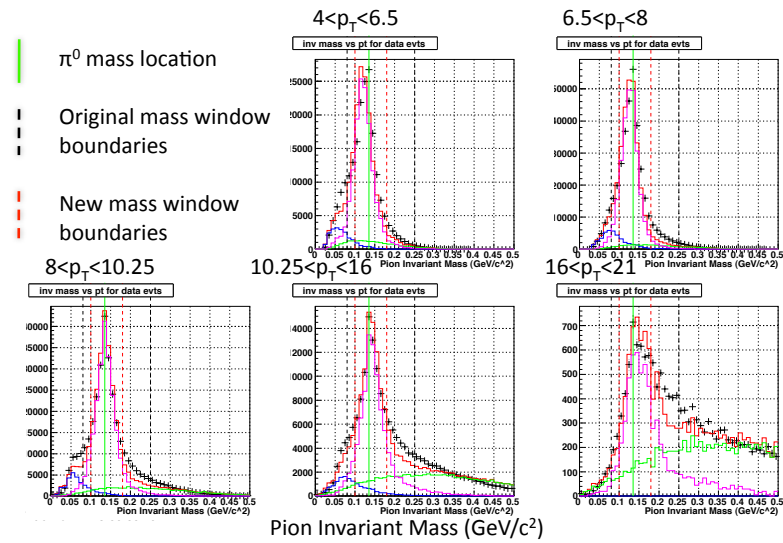
Data-Fit Comparison



10

Indicate location of peak and maybe mass window

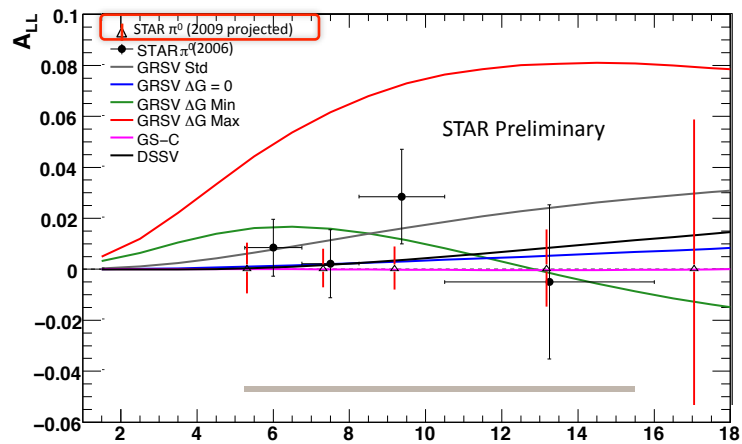
Varying Mass Windows



Assign a systematic to the underlying data-simulation discrepancy by examining how the A_{LL} depends on the mass window we choose to calculate it in.

Heavier lines?
 Try to get rid of grid
 Bigger x-axis labels

Projected Statistical Errors

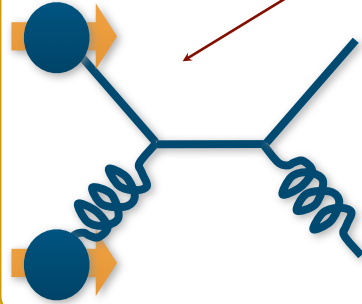


p_T bin	Systematic Errors				Statistical Errors
	Trigger Bias	Mass Window	Rel Lumi	Trans Component	
4-6.5	.00028	.0069	.0015	.00025	.015
6.5-8	.00059	.0024	.0015	.00025	.01
8-10.25	.00097	.0078	.0015	.00025	.012
10.25-16	.0017	.016	.0015	.00025	.022
16-21	.0068	.021	.0015	.00025	.11

I will only be showing projected statistical errors for the 2009 measurement: they're in red at 0. The 2006 result is shown in black, along with a bunch of theory curves: the two important ones are the black one, which is the best global fit result of delta g, and the red one, which shows the a_{ll} prediction for maximally polarized gluons. This grsv max prediction was disfavored by the 2006 result: with smaller errors from more data and an improved algorithm, we should be able to improve on the 2006 result. Thank you.

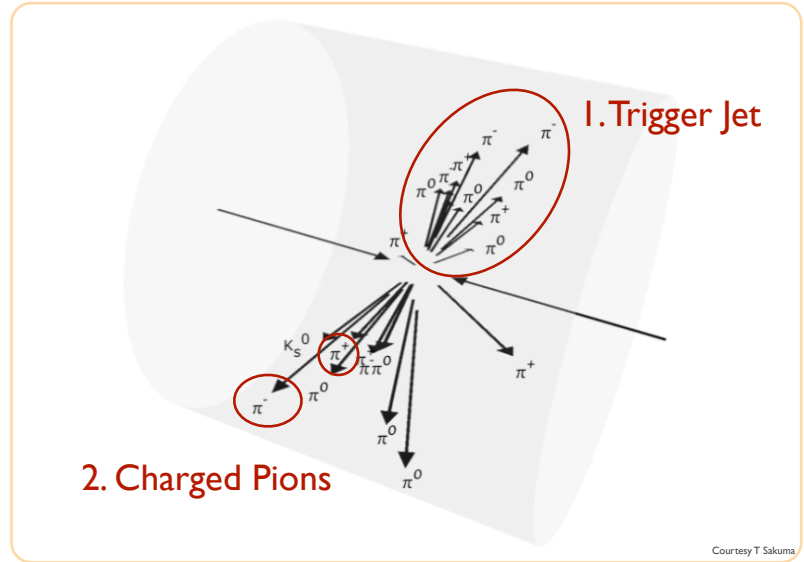
Kinematics

$$d\sigma^{pp \rightarrow h + jet X} = \sum_{f_1, f_2, f} \int dx_1 dx_2 dz f_1^{H_1}(x_1, \mu_{FI}^2) f_2^{H_2}(x_2, \mu_{FI}^2) \\ \times d\hat{\sigma}^{f_1 f_2 \rightarrow f X'}(x_1 p_1, x_2 p_2, p_h / z, \mu_{FI}, \mu_{FF}, \mu_R) D_j^h(z, \mu_{FF}^2) \times \mathcal{S}(p_i)$$



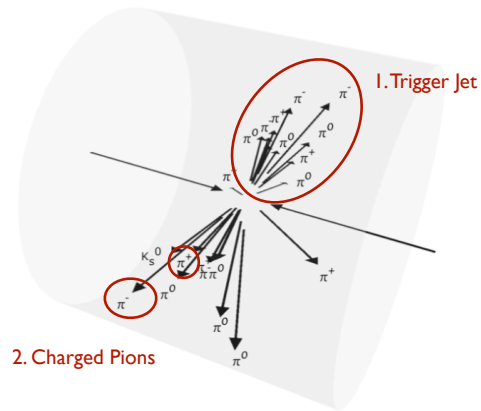
$$z \equiv \frac{p_T^h}{p_T^{jet}}$$

At high x and z , the pion preferentially probes the valence quark distribution. Thus A_{LL} goes like $\Delta q \Delta g$.



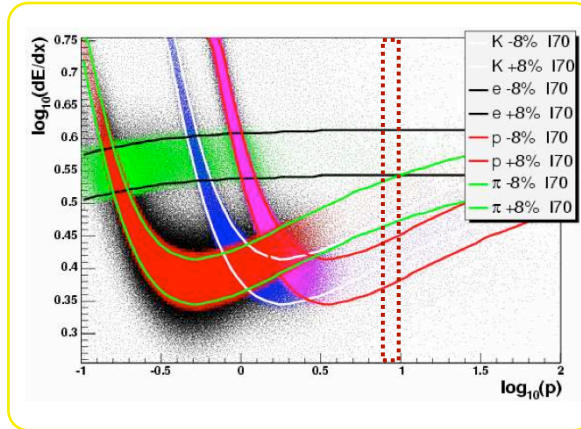
Courtesy T Sakuma

Event Details



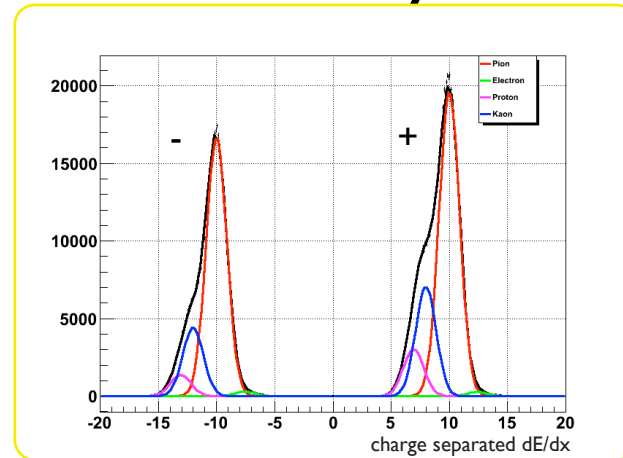
- Triggered by 5.4 GeV E_T deposited in 1×1 (η, ϕ)
- Jet found by midpoint cone with radius of 0.7
- Jet with $p_T > 10$ GeV/c
- Charged pions with $p_T > 2$ GeV/c on other side ($\Delta\phi > 2$)

Particle ID



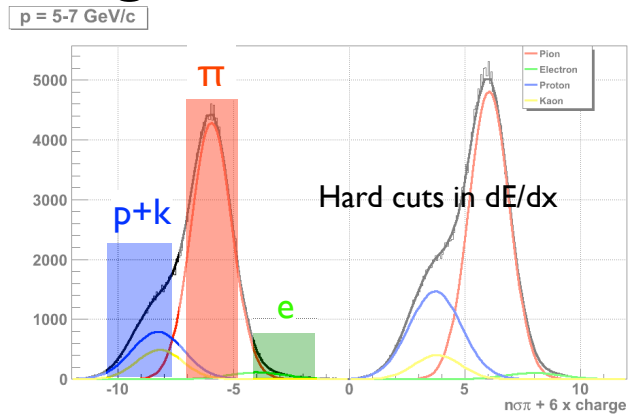
For a given momentum higher than MIP,
 dE/dx corresponds to particle mass.

Particle ID by dE/dx



Scaled dE/dx sorted by momentum
Constrained 8-Gaussian fit

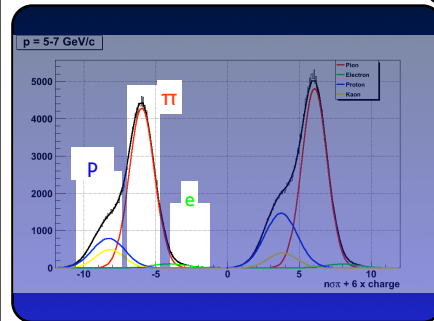
Background Subtraction



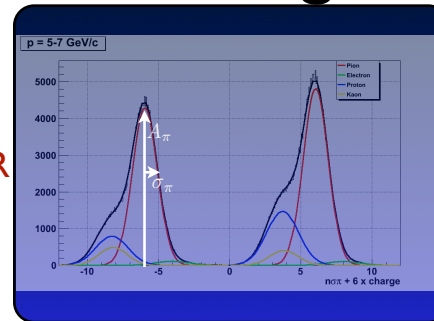
Background fraction and sideband A_{LL} determined

$$A_{LL}^{\pi} = \frac{A_{LL}^{RAW} - f'(p+k)A_{LL}^{(p+k)} - f'(e)A_{LL}^e}{1 - f'(p+k) - f'(e)}$$

PID: Fitting and Cutting

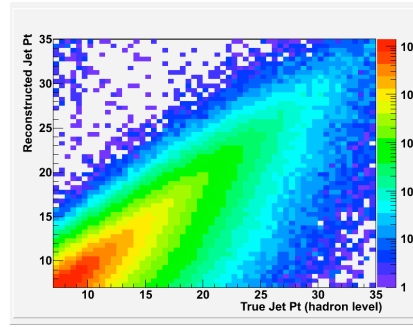


OR



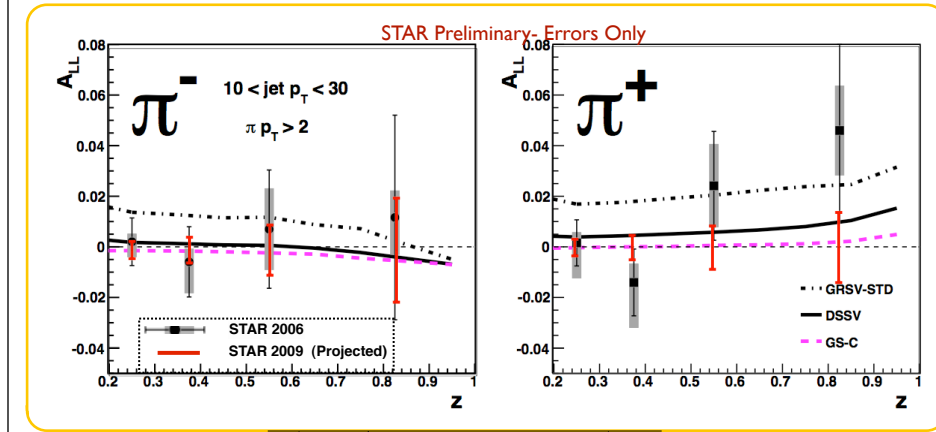
- Done with hard cuts and background subtraction.
- Compared to simple fitting.

Jet Unfolding



- “D’Agostini” iteratively generated unfolding matrix
- Monte Carlo over probabilistic unfolding scenarios

Projected Statistical Error



Z	Systematic Errors					
	PID	JES	Transverse	R3	Stat	
π^-	0.2-0.3	0.0021	0.0015	0.00025	0.0015	0.0029
	0.3-0.45	0.0025	0.0024	0.00025	0.0015	0.0046
	0.45-0.65	0.0064	0.0037	0.00025	0.0015	0.0095
	0.65-1.0	0.0041	0.0026	0.00025	0.0015	0.024
π^+	0.2-0.3	0.0002	0.0014	0.00025	0.0015	0.0029
	0.3-0.45	0.0034	0.0019	0.00025	0.0015	0.0046
	0.45-0.65	0.0054	0.0035	0.00025	0.0015	0.009
	0.65-1.0	0.0013	0.0057	0.00025	0.0015	0.022

Backup

Run 12 Predictions

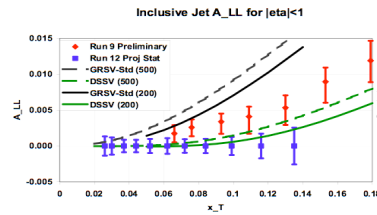


Figure 4.8: A_{LL} projections for inclusive jet measurements at 500 GeV in Run 12 data as function of x_T . The projections are compared with preliminary 200 GeV results from Run 9 and with NLO pQCD evaluations based on two commonly used sets of polarized parton distributions.

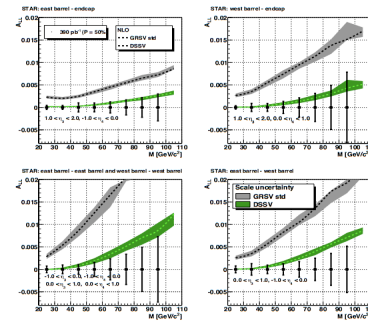


Figure 4.9: Projected A_{LL} for di-jet production for a large, multi-year, 500 GeV data set as function of the di-jet invariant mass M for different pseudo-rapidity regions.

190 pb⁻¹, 50% pol
 Dijet: multiyear, 390 pb⁻¹, 50% pol